Formation of dust in low-pressure magnetized hydrocarbon plasmas

2011 New J. Phys. 13 063006

(http://iopscience.iop.org/1367-2630/13/6/063006)

New Journal of Physics
The open-access journal for physics

Formation of dust in low-pressure magnetized hydrocarbon plasmas

L Laguardia[1,4], A Cremona[1], M De Angeli[1], E Lazzaro[1], S Ratynskaia[2], M Passoni[1,3], D Dellasega[1,3], G Gervasini[1], G Grosso[1], R Schiavone[1] and E Vassallo[1]

[1] Istituto di Fisica del Plasma 'P. Caldirola', CNR, Milan, Italy
[2] Royal Institute of Technology, Stockholm, Sweden
[3] NEMAS and Dipartimento di Energia, Politecnico di Milano, Milan, Italy
E-mail: laguardia@ifp.cnr.it

New Journal of Physics **13** (2011) 063006 (10pp)
Received 18 January 2011
Published 3 June 2011
Online at http://www.njp.org/
doi:10.1088/1367-2630/13/6/063006

Abstract. The rapid formation of large molecules and the subsequent production of solid-state dust particles in a low-pressure discharge is unlikely, because of the low rates of the polymerization reactions and short lifetimes of the species. Here, we suggest that C dust particles can form in atypically low (10^{-3} mbar)-pressure hydrocarbon plasmas if the dust charging time is much shorter than the gas residence time in the device; we present supporting experimental evidence for this. Such a condition can be obtained by the production of high-density plasmas. The results show that dust formation from the gaseous phase can occur in a much wider parameter range than is commonly assumed.

[4] Author to whom any correspondence should be addressed.

Contents

1. Introduction

Experiments devoted to the study of dust formation are typically performed in low-temperature radio-frequency (rf) discharges with low densities ($\sim 10^9\,\mathrm{cm}^{-3}$) and in the pressure range 10^{-2}–1 mbar [1–7]. For various applications and questions of principle, there is interest in understanding different plasma parameter regimes where dust can be formed. In the light of this, magnetized plasmas determine the conditions of access to wider pressure and plasma density ranges for dust growth. Namely, the presence of a magnetic field allows efficient plasma production, thanks to improved confinement or the use of resonant power absorption in combination with low neutral gas pressures.

Here, we report on the formation of C particles in the bulk of Ar–CH_4 plasmas in an unusually low ($\sim 10^{-3}$ mbar) pressure and high ($\sim 10^{11}\,\mathrm{cm}^{-3}$) density environment that is achieved by using a cusp magnetic trap.

Our main idea is that, for the formation of dust particles in a methane plasma, a key condition is that the dust charging time should be much shorter than the residence time of the reacting species in the containment volume. The neutral gas residence time in the volume V scales as $\tau_g = VP_g/\Gamma_g$, where Γ_g is the gas flow rate entering the volume and P_g is the gas pressure at room temperature. The charging rate of the dust particles (of radius a) is $\nu_{ch} \approx \omega_{pi}(a/\lambda_D)$ [8] and is therefore proportional to the plasma density, through the ion plasma frequency ω_{pi} and the Debye length λ_D.

The majority of experiments in which dust is produced are performed with a typical value of pressure of $\sim 10^{-1}$ mbar, a plasma density of $\sim 10^9\,\mathrm{cm}^{-3}$ corresponding to τ_g of several seconds [3] and $\tau_{ch} = 1/\nu_{ch}$ of a few ms. There is very little documentation available on dust formation in experiments performed at a much lower pressure.

In this paper, we show that the necessary condition, $\tau_{ch}/\tau_g \ll 1$, for the formation of nanodust grains can be obtained also in very low-pressure conditions if a high plasma density environment is produced, for instance using magnetic confinement. In the next section, we describe the experimental setup and diagnostic measurements used to investigate the conditions and major pathways of the nucleation of C dust particles. Our obtained results are consistent with a recent study on a novel diagnostic method of sub-micron dust based on the effect of dust on plasma fluctuation spectra [9, 10].

2. Experimental set-up

The experiments have been carried out in a magnetic cusp device, described elsewhere [11, 12], which allows the formation and confinement of high-density plasmas within its volume, evaluated as [13] $V_{\mathrm{cusp}} \approx \pi R^2 \rho_{\mathrm{L}}[\log(2R/\rho_{\mathrm{L}}) + 1]$, where R is the line cusp radius and ρ_{L} is the ion Larmor radius. The cusp magnetic field provides a magnetohydro-dynamic (MHD) stable confinement configuration by means of two identical solenoids fed by currents of the same intensity but opposite directions. The plasma is generated by rf breakdown at a point along the cusp where the local electron cyclotron frequency matches the frequency (2.45 GHz) of the rf source having a power of 350 W.

The neutral gas, a mixture of argon and methane, is fed through a mass flow controller that maintains a gas pressure (P_{g}) of 2×10^{-3} mbar under a flow rate (Γ_{g}) of about 0.45 $\mathrm{cm^3\,min^{-1}}$ (at 0 °C and 1 bar). With $R = 19$ cm and $B = 0.22$ T (at the line cusp), we have $\tau_{\mathrm{g}} \sim 130$ ms. The typical plasma parameters obtained are plasma density $n_i \sim 10^{11}\,\mathrm{cm^{-3}}$ and an electron temperature T_{e} of a few eV, while the ion temperature T_{i} equals the gas temperature [9, 10]. These parameter values guarantee the condition $\tau_{\mathrm{ch}}/\tau_{\mathrm{g}} \ll 1$ for particle sizes up to hundreds of nm.

The experimental device is equipped with a sample insertion system, used to introduce silicon wafer specimens that are subsequently subjected to an off-line surface analysis, and a mass spectrometer located along the line cusp, used to monitor the discharge. The diagnostics used include (i) atomic force microscope (AFM) and scanning electron microscope (SEM) analyses, which confirm the formation of spherical or polyhedrical nanosize particles; (ii) mass spectrometry for monitoring hydrocarbon molecules; (iii) Fourier transform infrared spectroscopy (FT-IR) for the *ex situ* study of the chemical composition of the particles; and (iv) optical spectroscopy for monitoring the plasma composition.

3. Results and discussion

3.1. Morphological analysis

Carbon dust particles have been characterized by AFM and SEM analyses of the Si wafers and are described in detail in [9]. Below we summarize the main findings:

1. Each grain can be viewed as an agglomerate (cluster) of nanospheres with a diameter of a few tens of nm, as can be seen in figure 1.
2. Dust grains with size around 20 nm up to clusters of 700 nm have been identified (see figure 3 of [9]).
3. Increasing the plasma exposition time leads to a greater number of larger, 500–700 nm width, clusters.
4. Energy dispersion x-ray spectroscopy has revealed the carbon composition of the particles.

3.2. Mass spectrometry

The composition of the residual gas flow in a methane/argon discharge is shown in figure 2. Apart from the dominant dissociation pattern of the source gas $\mathrm{Ar/CH_4}$, a clear production of mass 2 and masses in the range 26–30 is evident. Mass 2 is due to the formation of molecular

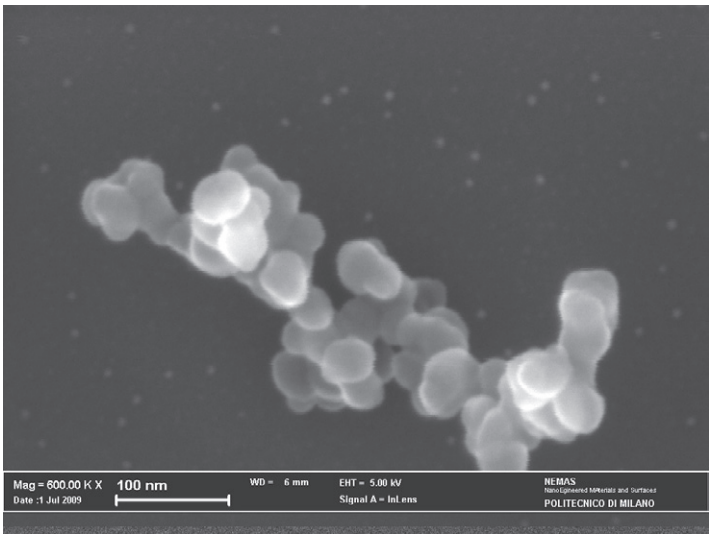

Figure 1. SEM image of a Si wafer exposed to a 25% methane mixture. The analysis was performed by a Zeiss Supra40 with Field Emission at 5 kV.

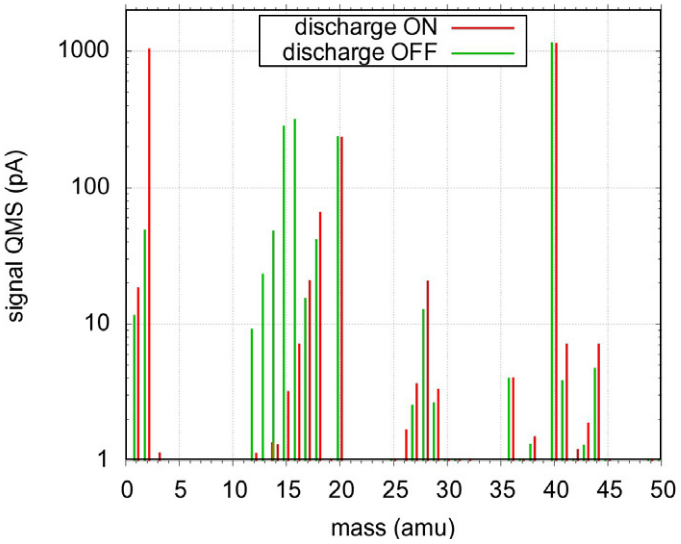

Figure 2. Mass spectrum recorded by a quadrupole mass spectrometer (QMS) before and during the discharge at a gas pressure of 2×10^{-3} mbar.

hydrogen (H_2), whereas mass 26 can be associated with the formation of acetylene (C_2H_2) in the discharge. Mass 28 can be attributed to both C_2H_4 and C_2H_6 having the main peak cracking pattern at this value. Moreover, the spectra show that the peaks of carbon-containing species leaving the discharge are lower than those in the working gas mixture. This means that a substantial portion of the carbon has been activated by plasma, by either dissociation or ionization processes, and has been condensed in dust particles, as shown by AFM and SEM analyses.

Furthermore, to confirm the interpretation of these observations, the experiment was repeated following the time evolution of the intensity of the mass spectrometer signal

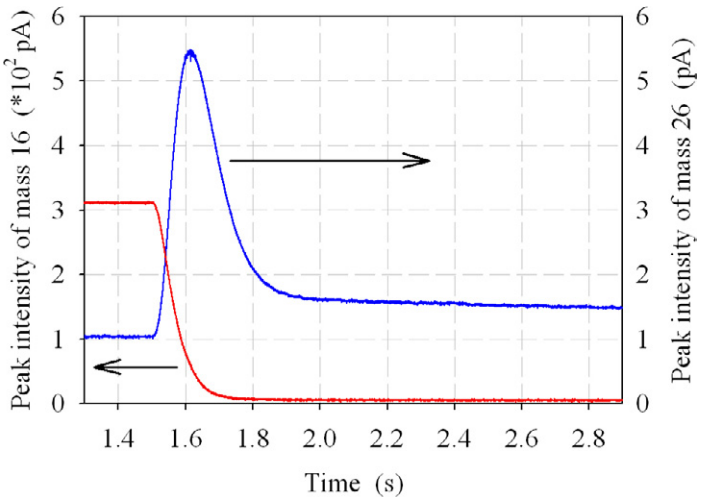

Figure 3. Time evolution of mass spectrometer signal of mass 16 (red line) and 26 (blue line) at a gas pressure of 2×10^{-3} mbar. The plasma was switched on at 1.5 s.

corresponding to masses 16 and 26 (i.e. CH_4 and C_2H_2). Figure 3 shows the behavior of the intensity after turning on the plasma source: the C_2H_2 signal has an overshoot that subsequently decays to the steady state, as shown in figure 2, whereas the CH_4 signal simply decays. The time to reach the steady state is less than a second. This behavior is in agreement with the observations of [3] and also [4]: the decrease in the signal of C_2H_2 indicates the gas consumption during particle growth.

3.3. Fourier transform infrared (FT-IR) spectroscopy of the solid phase

The chemical structure of dust particles collected on the silicon wafer during plasma discharge can be deduced from the FT-IR spectrum shown in figure 4. The main bonding type is sp^3 bonding. A stretching vibration of the C–C bond is present at 1100 cm^{-1}, while the signal at 610 cm^{-1} is due to C–C deformation.

The spectral band observed between 3000 and 2800 cm^{-1} is due to aliphatic groups. The first peak at 2593 cm^{-1} corresponds to the $-CH_3$ asymmetric stretching vibration mode. The peaks at 2918 and 2852 cm^{-1} are assigned to the $-CH_2$ asymmetric and symmetric stretching vibration modes, respectively, and the corresponding bending vibrations are observed at 1450 and 1370 cm^{-1}.

The presence of sp^2 alkene groups in the internal structure is evidenced by the stretching absorption at 1649 cm^{-1}; another contribution is observed through the $=CH$ bending mode at 963 cm^{-1}. The signal at 470 cm^{-1} is characteristic of the aliphatic cycle compound that is confirmed by the band at 886 cm^{-1}. The peak at 736 cm^{-1} is characteristic of the $-(CH_2)_3-$ functional groups. The peak at 1550 cm^{-1} is attributed to the C–O bond.

From these results it is possible to conclude that dust grains contain essentially carbon atoms bonded in random and ramified mode to other carbon atoms, sometime present also as rings.

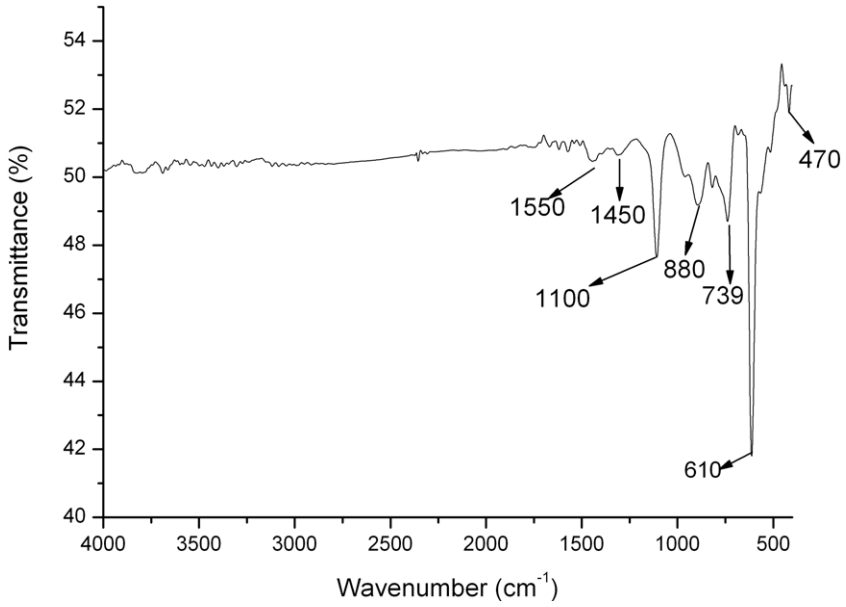

Figure 4. FT-IR spectrum of collected dust particles.

3.4. Optical emission spectroscopy (OES)

The plasma phase has been investigated by using optical emission spectroscopy in the 300–1000 nm spectral range. The spectra (figures 5 and 6) show the emission of CH (430 nm system), H_2 and H chemical moieties as a result the fragmentation of CH_4 molecules. The presence of C_2 Swan bands is due to from the dehydrogenation of hydrocarbon molecules (i.e. C_2H_2, C_2H_4 and C_2H_6) formed in the plasma phase. The higher intensity of atomic hydrogen lines as compared with molecular hydrogen is evidence of the high breaking rate of hydrogen molecules due to the fragmentation of CH_4 molecules and the dehydrogenation of hydrocarbon molecules.

3.5. Expected chemical processes

For the interpretation of the formation of dust particles in low-pressure plasmas, we relied on a vast body of literature [4], [14–20]. In the very-low-pressure experiments described here, we identify four main steps of the process:

1. The growth of large-molecule structures from molecular species in the gas phase.
2. Nucleation: this phase is the result of the development of large-molecule structures up to a given size for which the molecular edifices undergo an avalanche condensation process with a phase transition that leads to the formation of a solid core. A size of about 5 nm is expected for the first formed super small particles [14].
3. Coagulation: when the concentration of the first formed super-small particles increases up to a critical value, a coagulation process takes place, leading to the formation of spherical aggregates with a size of $\geqslant$ 10 nm of dust in a way similar to plasma experiments with SiH_4 [7, 18].
4. Finally, multiply charged particles aggregate further by surface radical attachment.

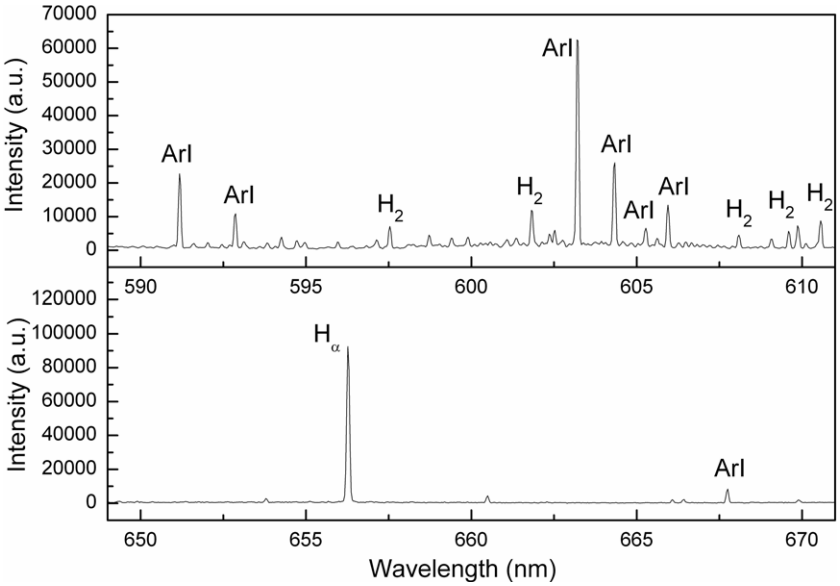

Figure 5. Optical emission spectra showing ArI, H_2 and H chemical species in the range 590–670 nm.

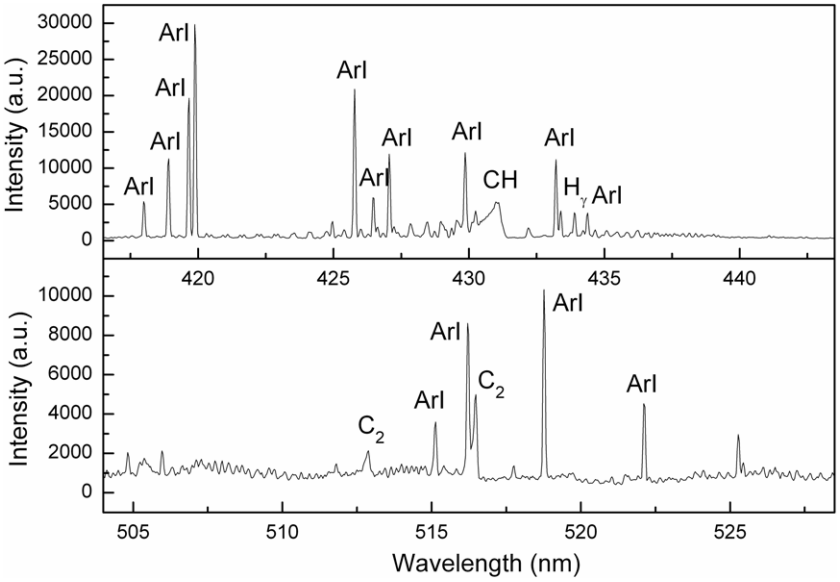

Figure 6. Optical emission spectra showing ArI, C_2, CH and H chemical species in the range 417–528 nm.

To describe the particle growth kinetics in the present experiment, a framework based on the general reaction mechanisms of hydrocarbon chemistry can be applied [16, 19]. The production of acetylenic compounds (C_2H_x) appears to be a key mechanism for the formation of dust particles in hydrocarbon plasmas [20, 21]. Electron attachment to acetylenic compounds and the subsequent ion-neutral reactions might lead to the production of high-mass carbon anions that are then trapped in the plasma, and finally ends in the formation of dust. For the

formation of solid particles in a methane plasma, the conversion of methane into acetylene is required.

We sought to optimize the experimental conditions for obtaining high electron density in order to improve the efficiency of methane conversion into acetylene (very low pressure, high power and high dilution in argon [22–25]). The main gas-phase products of methane conversion in plasma discharge are ethane, ethylene, acetylene, propane and hydrogen. In low-pressure conditions (i.e. low electron density), ethane is the most abundant product of fragmentation; thus the production of hydrogen is also relatively low. When the electron density increases, the products' distribution is shifted from ethane to ethylene and finally to acetylene, by a subsequent dehydrogenation reaction, with an increase in atomic hydrogen [26]. Evidence is provided by optical spectroscopy and mass spectrometry that there is a significant increase in H_2 compatible with the conversion of methane into acetylene. In this paper, we provide a description of the plasma chemical processes.

The initial reaction is hydrogen extraction from methane by collision with energetic electrons, leading to the formation of CH_3, CH_2 and CH radicals. According to ([15], [27–30]), these processes can be considered most probable judging from the corresponding reaction rates.

CH_2 and CH are produced also by secondary radical dissociation. CH_3 and CH_2 radicals are involved in chemical reactions that lead to the formation of C_2H_6 species according to the following molecular processes, displayed with the corresponding coefficient $\log_{10} A$ of the Arrhenius reaction rate $k_f = A(T/k_B)^b \exp(-E_a/k_B T)$, at a fixed temperature T and pressure [2, 28] (the exponent b is dimensionless and $k_B = 8.618 \times 10^{-5}\,\mathrm{eV\,K^{-1}}$ is the Boltzmann constant; E_a is the threshold energy; the units of the reaction rate factor A are consistent with a reaction rate in $\mathrm{mol\,cm^{-3}\,s^{-1}}$ [28]),

$$\mathrm{CH_2 + CH_4 \rightarrow 2CH_3}, \quad \log_{10} A = 5.2, \tag{1}$$

$$\mathrm{CH_3 + CH_3 \rightarrow C_2H_6}, \quad \log_{10} A = 26.1, \tag{2}$$

while CH radicals can react with CH_4 molecules and form C_2H_4 according to the chemical reaction [28]

$$\mathrm{CH_1 + CH_4 \rightarrow C_2H_4 + H}, \quad \log_{10} A = 13.5. \tag{3}$$

The chemical species C_2H_6 resulting from reactions (1) and (2) produce C_2H_4 molecules through electron impact according to a reaction having high probability because of the low threshold energy [29],

$$\mathrm{C_2H_6 + e \rightarrow C_2H_4 + H_2 + e}, \quad E_a = 1.41\,\mathrm{eV}. \tag{4}$$

The ethylene molecules formed as a consequence of reactions (3) and (4) are converted by electron impact into acetylene [29],

$$\mathrm{C_2H_4 + e \rightarrow C_2H_2 + H_2 + e}, \quad E_a = 1.81\,\mathrm{eV}. \tag{5}$$

The reaction path outlined above is consistent with the observed presence of acetylene determined by the mass spectrometer. The dissociative attachment of C_2H_2 leads to the formation of C_2H^- ions according to the reaction [15, 28]

$$\mathrm{2\,C_2H_2 + 2e \rightarrow 2\,C_2H^- + H_2}, \quad E_a = 1.66\,\mathrm{eV}. \tag{6}$$

A subsequent polymerization leads to the production of macromolecules C_nH_m through ion–molecular reactions of the C_2H^- anion with either CH_4 or C_2H_2. Here, subscripts n and m

represent the number of monomer units in polymer fragments. Note that for polymerization, ion–molecular reactions are dominant (faster) over ion–ion recombination. However, when the particle size reaches a critical value, the ion–ion recombination becomes important and eventually stops the chain reaction of polymerization.

After the formation of the first super-small particles, the necessary condition for the coagulation stage to take place is that the electron attachment time, τ_e, is much shorter than the gas residence time, $\tau_e \ll \tau_g$. The electron attachment time scale can be estimated from the dust charging frequency ν_{ch} given above ($\tau_e \approx \tau_{ch}$). With the plasma parameters of the order of magnitude as discussed in Section 2, we have typically for $a \sim 10$ nm an estimate of $\tau_e \sim 0.1$ ms, which is well below $\tau_g \sim 130$ ms.

Values of τ_e that are two or three orders of magnitude smaller than τ_g are made possible by the use of magnetic confinement and plasma production using electron cyclotron resonance, which provide high, $\sim 10^{11}\,\mathrm{cm}^{-3}$, density compared to the more typical $\sim 10^{9}\,\mathrm{cm}^{-3}$ in usual discharges.

The final stage of the process of formation of dust particles by agglomeration requires an increase in the density of primary aggregates. This description is in agreement with the results of surface analysis of the wafers. The dust particle size detected by AFM and SEM analyses is in the range from ~ 25 nm for single grains of apparently polyhedrical grains to micron-sized agglomerates.

This appears consistent with recent dust formation models [31] that predict that the final dimension distribution of larger dust particles (cluster-like) during the process of agglomeration depends on the dimensions of the aggregates that have grown in the previous phase. The agglomeration phase can occur with enhanced probability, by a process of polarization of the larger particles by the field of the smaller ones, only when the original aggregates' effective radius a is larger than a certain critical value, solving the implicit relation

$$a_\star = \left[\frac{n_i}{n_d}\frac{\sigma_0}{\pi}(1-P)\right]^{1/2}\sqrt{\zeta}\exp(-1/2\zeta). \tag{7}$$

According to Olevanov *et al* [31], $\sigma_0 \sim 0.5 \times 10^{-14}\,\mathrm{cm}^2$ is the cross-section for the interaction of ions with neutral gas atoms. In equation (7), $\zeta = a_\star k T_i / Z_d Z_i e^2$ is the ratio of the dust grain thermal energy to the electrostatic energy, which is always very small. Then the evaluation $a_\star$ is performed considering that both $\zeta \ll 1$ and also $P = n_d Z_d / n_i \ll 1$ where n_d, n_i, Z_d and Z_i are the dust and ion densities and charge numbers. For the present experimental conditions, the critical radius can be estimated, by using equation (7), to be 10 nm. The information obtained from the FT-IR spectrum is that the chemical composition of dust is polymer-like carbon, which is in agreement with the formation process suggested.

4. Conclusion

The process of formation of solid carbon-based particles in the bulk of an atypical low-pressure magnetized plasma has been experimentally proved and confirmed by repeated experiments, and it has been interpreted in terms of the favorable conditions provided by a confinement time much longer than the time of the charging of the precursor particles. The results presented here complement the observations obtained with a novel *in situ* diagnostic technique based on the effect of dust on plasma fluctuations [9, 10].

Acknowledgment

The authors acknowledge support from MIUR (Ministero dell'Universitàe della Ricerca) under grant number PRIN-2007L4YEW4.

References

[1] Berndt J, Hong S, Kovacevic E, Stefanovic I and Winter J 2003 *Vacuum* **71** 377
[2] Stoykov S, Eggs C and Korsthagen U 2001 *J. Phys. D: Appl. Phys.* **34** 2160
[3] Hong S, Berndt J and Winter J 2003 *Plasma Source Sci. Technol.* **12** 46
[4] Consoli A, Benedikt J and Von Keudell A 2009 *Plasma Source Sci. Technol.* **18** 034004
[5] Selwyn G S, Weiss C, Sequeda F and Huang C 1998 *Thin Solid Films* **317** 85
[6] Stoffels E, Stoffels W, Kersten H, Swinkels G and Kroesen G 2001 *Phys. Scr.* **T89** 168
[7] Mikikian M, Cavarroc M, Couedel L, Tessier Y and Boufendi L 2010 *Pure Appl. Chem.* **82** 1273
[8] De Angelis U, Capobianco G, Marmolino C and Castaldo C 2008 *Plasma Phys. Control. Fusion* **48** B91
[9] Ratynskaia S, De Angeli M, Lazzaro E, Marmolino C, De Angelis U, Castaldo C, Cremona A, La Guardia L, Gervasini G and Grosso G 2010 *Phys. Plasmas* **17** 043703
[10] Ratynskaia S, De Angeli M, De Angelis U, Marmolino C, Capobianco G, Lontano M, Lazzaro E, Morfill G and Gervasini G 2007 *Phys. Rev. Lett.* **99** 75002
[11] Gervasini G, De Angeli M, Amedeo P and Schiavone R 2007 *Fusion Sci. Technol.* **51** T2334
[12] Spinicchia N, Angella G, De Angeli M, Gervasini G and Signorelli E 2006 *Surf. Coat. Technol.* **200** 6434
[13] Miyamoto K 1980 *Plasma Physics for Nuclear Fusion* (Cambridge: MIT Press) section 16.6
[14] Perrin J and Hollenstein C H 1999 Dusty plasmas: between science and technology *Source and Growth of Particles* ed A Bouchoule (New York: Wiley) chapter 2 566–70
[15] De Bleecker K, Bogaerts A and Goedheer W 2006 *Phys. Rev.* E **73** 026405
[16] Kobayashi H, Bell A T and Shen M 1974 *Macromolecules* **7** 277
[17] Doyle J R 1997 *J. Appl. Phys.* **82** 4763
[18] Goedheer W J and De Bleecker K 2005 *Proc. 4th Int. Conf. on Atomic and Molecular Data and their Applications (ICAMDATA2004) (Toki, Japan, 2005)* (*AIP Conf. Proc.* **771** 118)
[19] Tibbitt J M, Jensen R, Bell A T and Shen M 1977 *Macromolecules* **10** 647
[20] Winter J and Leukens A 1999 *Proc. 14th Int. Symp. on Plasma Chemistry (ISPC14) (Prague)* vol 4 (Prague: Institute of Plasma Physics, Academy of Science of the Czech Republic) 2199
[21] Deschenaux Ch, Affolter A, Magni D, Hallenstein Ch and Fayet P 1999 *J. Phys. D: Appl. Phys.* **32** 1876
[22] Schulz-von der Gathen V, Röpcke J, Gans T, Käning M, Lukas C and Döbele H F 2001 *Plasma Source Sci. Technol.* **10** 530
[23] Heintze M, Magureanu M and Kettlitz M 2002 *J. Appl. Phys.* **92** 7022
[24] Sergey Y. Savinov, Hwaung L, Hyung K S and Byung-Ki N 2004 *Korean J. Chem. Eng.* **21** 601
[25] Riccardi C, Barni R, Fontanesi M and Tosi P 2000 *Chem. Phys. Lett.* **329** 66
[26] Oumghar A, Legrand J C, Diamy A and Turillon N 1995 *Plasma Chem. Plasma Process.* **15** 87
[27] Kline L E, Partlow W D and Bies W E 1989 *J. Appl. Phys.* **65** 70
[28] Masi M, Cavallotti C and Carrà S 1998 *Chem. Eng. Sci.* **53** 3875
[29] Morrison N A, William C and Milne W I 2003 *J. Appl. Phys.* **94** 7031
[30] Suib S L and Zerger R P 1993 *J. Catal.* **139** 383
[31] Olevanov M A, Mankelevich Y A and Rakhimova T V 2003 *Tech. Phys.* **48** 1270